Energy Conversion and Management 253 (2022) 115147

Contents lists available at ScienceDirect

Energy Conversion and Management

journal homepage: www.elsevier.com/locate/enconman

Multi-objective bi-level quantity regulation scheduling method for electric-thermal integrated energy system considering thermal and hydraulic transient characteristics

Su Guo [a,*], Guotao Song [a], Mengying Li [b], Xiaohui Zhao [c], Yi He [a], Ainur Kurban [a], Wenjia Ji [a], Jiale Wang [a]

[a] College of Energy and Electrical Engineering, Hohai University, Nanjing, China
[b] Department of Mechanical Engineering & Research Institute for Smart Energy, The Hong Kong Polytechnic University, Hong Kong Special Administrative Region
[c] Northwest Electric Power Design Institute Co., Ltd. of China Power Engineering Consulting Group, China

ARTICLE INFO

Keywords:
Integrated energy system
Quantity regulation
Bi-level scheduling method
Multi-objective optimization
Thermo-hydraulic dynamic model
Mixed integer nonlinear programming

ABSTRACT

In most studies about operation optimization of integrated energy system (IES), the heating subsystem adopts the quality regulation method. However, considering the poor economy of quality regulation, quantity regulation method is proposed to improve the economy. Due to possible hydraulic vertical imbalance resulted from quantity regulation, the operation optimization must consider the effects of both thermal and hydraulic dynamic characteristics on IES. In this work, a new multi-objective quantity regulation scheduling method of electric-thermal IES is proposed, which adopts an electro-thermal decoupling bi-level optimization structure, a nonlinear dynamic thermo-hydraulic network model, objectives of economy and carbon emission indices and more reasonable nonlinear constraints. An IES prototype of 5-node power system with 5-node thermal system is designed to verify the proposed quantity regulation scheduling method. When solving the optimization problem, method NSGA-II combines with Gurobi is 40% faster in computational speed when compared with other methods. When compared with a single layer solution method, the proposed bi-level optimization model results in a scheduling strategy that can absorb 100% renewable power with operation cost of 10150.18 U.S. dollars (39.5% reduction) and carbon emission of 1303.7 ton (13% reduction). The hydraulic transient process resulted from the quantity regulation is also analyzed to demonstrate that the optimized scheduling strategy could satisfy the safety requirement of the heating network operation. Therefore, the proposed scheduling optimization method is more effective and satisfied.

1. Introduction

Integrated energy system (IES) is a comprehensive solution for multi-energy production, transmission and utilization that can effectively boost the renewable energy utilization rate and reduce carbon emissions [1–3]. Recent research progresses about IES modeling, planning and operation optimization are investigated and summarized as follows.

(1) Planning and operation optimization

The conventional planning and/or operation optimization on IES is treated as a mixed integer linear programming (MILP) problem, and the solution can be mainly categorized twofold: numerical method and heuristic algorithm [4]. With more factors considered in IES, the optimization gradually switches from MILP to mixed integer nonlinear programming (MINLP). The numerical method can accurately obtain the optimal solution for MILP. However, for MINLP, the nonlinear constraints must be linearized, which will compromise the accuracy of results. Heuristic algorithm can be used to solve both MILP and MINLP, but the accuracy is difficult to guarantee [5]. Therefore, the IES is layered in some studies, and the system model is divided into several simpler subsystems. In each layer, the optimization method is applied independently to obtain the optimal results, and the global optimal solution is obtained through the information exchange between the layers. The number of layers is usually 2 when computational efficiency is taken into consideration. For example, Kong et al. proposed a bidding based bi-level multi-time scale scheduling method for multi-operator virtual power plants [6]. Ju et al. proposed a bi-level stochastic scheduling optimization method for virtual power plants of wind power/

* Corresponding author.
E-mail address: guosu81@126.com (S. Guo).

https://doi.org/10.1016/j.enconman.2021.115147
Received 26 September 2021; Received in revised form 2 December 2021; Accepted 14 December 2021
Available online 22 December 2021

Nomenclature

Abbreviations

CHP	Combined Heat and Power
DHS	District Heating System
DPS	District Power System
EB	Electric Boiler
PV	Photovoltaic
TES	Thermal Energy Storage
WT	Wind Turbine
IES	Integrated Energy System

Indices

k	iterative times
i	pipe number
j	node number
t	calculation time

Parameters and constants

a	propagation velocity of water hammer wave
C_p	hot water specific heat capacity
f_{PV}	derating factor of PV
f_{pipe}	frictional resistance coefficient of pipe
g	gravitational acceleration
p_{gas}	price of natural gas per unit volume
v_{in}	cut-in wind speed
v_{out}	cut-out wind speed
v_r	rated wind speed
A_{pipe}	cross-sectional area
$G_{T,STC}$	radiation intensity in the laboratory test
$H_{eb}^{min}, H_{eb}^{max}$	minimum and maximum output thermal power of EB
$P_{chp}^{min}, P_{chp}^{max}$	minimum and maximum output power of CHP
c_{device}	unit operation cost of various devices
P_{RPV}	rated output power of PV
P_{RWT}	rated output power of WT
R	total thermal resistance
$R_{chp}^{down}, R_{chp}^{up}$	down and up ramping limits of CHP
$R_{eb}^{down}, R_{eb}^{up}$	down and up ramping limits of EB
T_a	ambient temperature
$\alpha_1, \alpha_2, \alpha_3$	carbon intensity coefficients of CHP
$\beta_1, \beta_2, \beta_3$	carbon intensity coefficients of coal-fired plant
φ_1, φ_2	coefficient representing the pump characteristic curve
λ	low calorific value of natural gas
η_{eb}	efficiency of EB
ρ	hot water intensity
ε	preset tolerance value
$\boldsymbol{A_H}$	node-branch incidence matrix
$\boldsymbol{A_r}$	reduced node-branch matrix
$\boldsymbol{B_f}$	loop-branch matrix
$\boldsymbol{K}$	pipe resistance vector

Variables

H_{device}^t	output electrical power of device
H_{node}^j	thermal power in node
H_{pipe}	piezometric head of pipe
m_{pipe}	mass flow in pipe
P_{device}^t	output electrical power of device
Q_{pipe}	volume flow in pipe
Q_{tes}^t	heat storage of TES
T_{pipe}	temperature of pipe
T_{node}^j	node temperature
V_{gas}^t	natural gas volume consumed by CHP
α_{chp}^t	heat-to-electric ratio of CHP
η_{chp}^t	electrical efficiency of CHP
δ_{chp}^t	load rate of CHP
$\boldsymbol{m_{pipe}}$	mass flow vector in pipe
$\boldsymbol{m_{node}}$	mass flow vector in node

photovoltaic/energy storage system considering the uncertainty and demand response [7]. Both of the aforementioned studies improve the economy of the system. Similarly, The bi-level scheduling optimization method is applied to the optimization of reducing the carbon emission from IES [8,9]. The bi-level optimization method can also be applied to the stochastic robust optimization of energy system, and the reliability of the optimization results can be improved [10,11]. These studies demonstrate the advantages of bi-level optimization, which is used in this work. Considering the complexity of bi-level optimization, several advanced solution methods have been introduced, including Karush-Kuhn-Tucher-(KKT) based methods [8–10] and iterative calculation based on heuristic algorithm [6,11].

For the optimal objective of scheduling in IES, economy is the primary consideration. The economic scheduling model of IES considering power grid, heating network and gas network has been extensively studied [12]. For example, an operation strategy of community IES considering unit combination is proposed in [13] based on the economic objective. In addition to economy, indicators like environmental impact are also taken as optimization objectives recently. Zhou et al. [14] propose a new deviation satisfaction strategy based on economy and carbon emission, which is applied to the planning and scheduling of gas/wind/photovoltaic/hydrogen IES. Sanaye et al. [15] introduce the exergy and economic optimization of a solar power generation system with traditional photovoltaic (PV) and centralized cooling/heating/power system. In [16], a multi-objective optimization model for both investment planning and operational management of distributed heating system is proposed, and the evolutionary algorithm is used to solve the optimization. Fonseca et al. [17] present the multi-objective optimization model with economy, environmental impact, social benefits, and the sustainability dimensions as objectives, and multi-objective algorithm NSGA-II is adopted to solve the optimization. Xu et el. [18] propose an optimal scheduling strategy that fully considers the contribution of wind farms, solar plants and coal-fired power plants to determine the balance of economic benefits and environmental impacts brought by a hybrid power generation system under natural constraints. Two objectives are transformed into a single objective and commercial solver LINGO is applied. Asl et al. [19] optimize the electrical/thermal/natural gas IES with economic, energy loss and three voltage unbalanced coefficients as objectives, and employ the modified teaching–learning based optimization (MTLBO) algorithm for optimization. In [20], a two-objective mixed integer nonlinear programming model is established, which considers the economic and environmental objectives calculated by life cycle analysis, and the overall objective is defined as the weighted sum of a single objective, which solved by commercial solver CPLEX. A multi-objective optimization model is established in [21] to optimize the operation cost, carbon emission and energy loss of an anaerobic digester considering the dynamic thermal effect and the uncertainty of wind and solar resources. Concurrently, a multi-task algorithm is designed to solve multiple IES optimizations. The operation optimization model of multi-objective two-stage electric-gas IES is presented in [22], NSGA-II is used to solve the multi-objective economic-environmental optimization model of the power system in the outer layer, and GA is used for the economic optimization of natural gas system in the inner layer. Zhang et al. propose a modeling method based on a novel energy cell with full

Table 1
Summary of selected literature about multi-objective optimization.

Reference	Optimization type	Objective function	Method/ Commercial solver
Fonseca et al. [17]	Design optimization	Economic Environmental	NSGA-II
Xu et al. [18]	Scheduling optimization	Economic Environmental	Multi-objective to single objective LINGO
Asl et al. [19]	Design optimization	Economic Energy loss Unbalance coefficients	MTLBO
Algieri et al. [20]	Design optimization	Economic Environmental	Multi-objective to single objective CPLEX
Wu et al. [21]	Scheduling optimization	Economic Environmental Energy loss	MO-MFEA-II
Song et al. [22]	Scheduling optimization	Economic Environmental	NSGA-II GA
Zhang et al. [23]	Scheduling optimization	Scheduling optimization	HNSGA-II
Wu et al. [24]	Scheduling optimization	Economic Performance index	NSGA-II with CDP
This work	Scheduling optimization	Economic Environmental	NSGA-II and Gurobi

duplex and multi-energy carrier coupling interaction, and propose a two-stage multi-objective optimal scheduling strategy [23]. The aforementioned literatures are summarized in Table 1.

In this work, we aim to reduce both the emission from burning natural gas and the operation cost of offshore micro IES (including the penalty cost of carbon emission). Therefore, we propose a bi-objective optimal scheduling model of offshore micro IES and the operation state of Gas Turbine Generator Unit (GTGU) considering the overall operation cost. NSGA-II is selected for optimization together with constraint dominated principle (CDP) [24]. Table 1 shows that the multi-objective optimization considering economy and environmental protection is widely used in IES. Furthermore, the solving methods are different. It can be roughly divided into two categories, heuristic algorithms and commercial solvers. Heuristic algorithms can directly solve the proposed model, and the commercial solvers need to linearize the constraints and transform the objective function into a single objective.

It is worth mentioning that most of the above operation optimization strategies considering heat supply are based on quality regulation, which adjusts the temperatures at the heat sources to meet the load demand and operate in the high mass flow range for a long time. However, the quality regulation is simple but uneconomic. In contrary, quantity regulation meets the load demand by regulating the mass flow, which can greatly improve the system economy [25]. However, the operation of quantity regulation is more complex, and frequent regulation of the mass flow in the pipeline will inevitably lead to serious hydraulic transient vertical changes. Severe hydraulic transient changes are undesirable to the safe operation of the pipe network, so it is also crucial to study the hydraulic transient change of the pipe network, to ensure the safe operation of the pipe network under the specified scheduling plan.

(2) Modeling of IES and its heating subsystem

In the heating subsystem of IES, the more economic quantity regulation needs more comprehensive dynamic models. The mathematical model of IES has become more comprehensive with the progress of research. For the early energy hub or energy bus model, it simply describes the relationship between the input and output of IES. Its boundary only considers the match of equipment output and load demand, while the internal energy flow transfer process is ignored. Nowadays, every transmission network is gradually considered in IES, which improves the accuracy of scheduling strategy [26]. The research of energy network is mainly based on the power grid, the heat network and the natural gas network, where the steady-state model of each

Table 2
Summary of selected literature about heating network model in IES.

Reference	System composition	Heating network model	Regulation mode	Hydraulic transient characteristics
Lu et al. [27]	Thermal-electrical	steady-state	quantity regulation	N
Luo et al. [28]	Thermal-electrical	steady-state	quantity regulation	N
Dancker et al [30]	Thermal	steady-state	quantity regulation	N
Qin et al. [32]	Thermal-electrical	Quasi-dynamic (steady-state hydraulic and dynamic thermal)	quantity regulation	N
This work	Thermal-electrical	dynamic hydraulic and dynamic thermal	quantity regulation	Y

network is the mainstream. Lu et al. consider the heat transfer model of pipe network in the study of IES scheduling strategy, and the results show that the pipe network system can improve the flexibility of system operation [27]. In [28], the steady state model of IES including source, network and load is established, while the interaction among source, network and load is considered in the operation optimization. Gu et al. use the thermal inertia of heat supply network and buildings in the IES to absorb more wind power [29]. The above studies adopt the heat loss model regardless of the transmission delay of the heating network. Although the heat loss model can present the results of heat transfer, it fails to present the process of heat transfer. Therefore, researches on the dynamic characteristics of heating network have been conducted. Dancker et al. add time delay to the traditional static heat supply network model, and use an improved Newton-Raphson iterative algorithm to solve both the hydraulic steady model and the thermal quasi-dynamic model, which improve the calculation accuracy [30]. Yao et al. transform the partial differential equation of heat transfer into linear equality constraint by using finite element difference method, and then develop the dynamic power flow model of electric-thermal IES [31]. Similarly, according to the partial differential equation of dynamic heat transfer, Qin et al. combine the finite element difference method with Newton-Raphson iterative algorithm to propose a generalized quasi-dynamic model of distributed energy electro-thermal IES [32]. The above literatures strive to incorporate the dynamic characteristics of heat network into IES by different methods. Table 2 summaries the above researches using quantity regulation, which demonstrates that both the steady-state hydraulic model and dynamic thermal model are used in latest research. However, it is essential to consider the hydraulic dynamic characteristics into operation to avoid possible operation safety problems such as hydraulic vertical imbalance.

Based on the above literature review, for electric-thermal integrated energy system, the research gaps that will be filled in this work are: (1) develop an efficient scheduling method based on quantity regulation; (2) establish a hydraulic dynamic model of heat network. Specifically, the main contents of this paper that are originated from the research gaps are:

(1) A multi-objective bi-level quantity regulation scheduling method for electric-thermal integrated energy system is proposed, and both the economy and the carbon emission are chosen as optimization objectives.
(2) The thermal and hydraulic dynamic models of heating network in IES are established, and it is incorporated into the multi-objective bi-level optimal scheduling process.
(3) Combined with the efficient heuristic multi-objective algorithm NSGA-II and numerical solver Gurobi, a new multi-objective

Table 3
Parameters of devices.

Unit	P_{min}(kW)	P_{max}(kW)	Up ramp	Down ramp	Unit generation cost ($/MW)
Coal-fired	0	30,000	9000	9000	0.015
WT	0	–	–	–	0.008
PV	0	–	–	–	0.001
CHP	0	15,000	4500	4500	0.014
EB	0	15,000	4500	4500	0.0018
TES	0	15,000	–	–	0.0016

double-layer solution method is developed, and the optimal Pareto front can be obtained quickly and accurately.

(4) The hydraulic transient process caused by the quantity regulation of the IES is analyzed, which provides useful information for the safe operation of the IES.

The rest of the paper is organized as follows: The dynamic modeling of devices and heating network in IES are presented in Section 2. Bi-level multi-objective optimization including structure, model and solution method are presented in Section 3. The results and discussion including comprehensive performance comparisons of multi-objective bi-level evolutionary algorithms, quantitative economic-environmental comparison of different IES technologies, cost and energy production breakdown, power output analysis, dynamic thermal energy flow and hydraulic transient process analysis are presented in Section 4. Finally, the conclusions are presented in Section 5 (Table 3).

2. Modeling of electric-thermal integrated energy system

As shown in Fig. 1, the considered electric-thermal IES includes three parts: multi-objective decision-making center, energy supply system and consumers. The multi-objective decision center selects the most suitable decision for dealers according to the selected objectives. The energy supply system includes energy production devices and energy transmission networks. Energy production devices generate different forms of energy and transmit them to consumers through the transmission networks to meet different load needs. In this part, the models of devices considering operation characteristics, and thermal and hydraulic dynamic models of heating network are established.

2.1. Models of the power and heat generation units

(a) CHP unit

CHP unit utilizes the natural gas to generate heat and electricity. In practice, the efficiency of CHP varies with load rate, and the heat-to-electric ratio is also expressed as a function of load rate [33].

$$P^t_{chp} = V^t_{gas}\lambda\eta^t_{chp} \tag{1}$$

$$H^t_{chp} = P^t_{chp}\alpha^t_{chp} \tag{2}$$

$$\eta^t_{chp} = 0.06(\delta^t_{chp})^4 - 0.12(\delta^t_{chp})^3 - 0.15(\delta^t_{chp})^2 + 0.45\delta^t_{chp} + 0.1 \tag{3}$$

$$\alpha^t_{chp} = 4.30\left(\delta^t_{chp}\right)^2 - 6.71\delta^t_{chp} + 4.22 \tag{4}$$

where λ is the low calorific value of natural gas, P^t_{chp} and H^t_{chp} are the output electricity and heat in period t, V^t_{gas} is the natural gas volume consumed by CHP. η^t_{chp} , α^t_{chp} and δ^t_{chp} are the electrical efficiency, heat-to-electric ratio and the load rate, respectively.

(b) Electric boiler

As an important electricity-to-heat equipment, electric boiler can absorb more renewable energy power in systems with high renewable energy penetration.

$$H^t_{eb} = P^t_{eb}\eta_{eb} \tag{5}$$

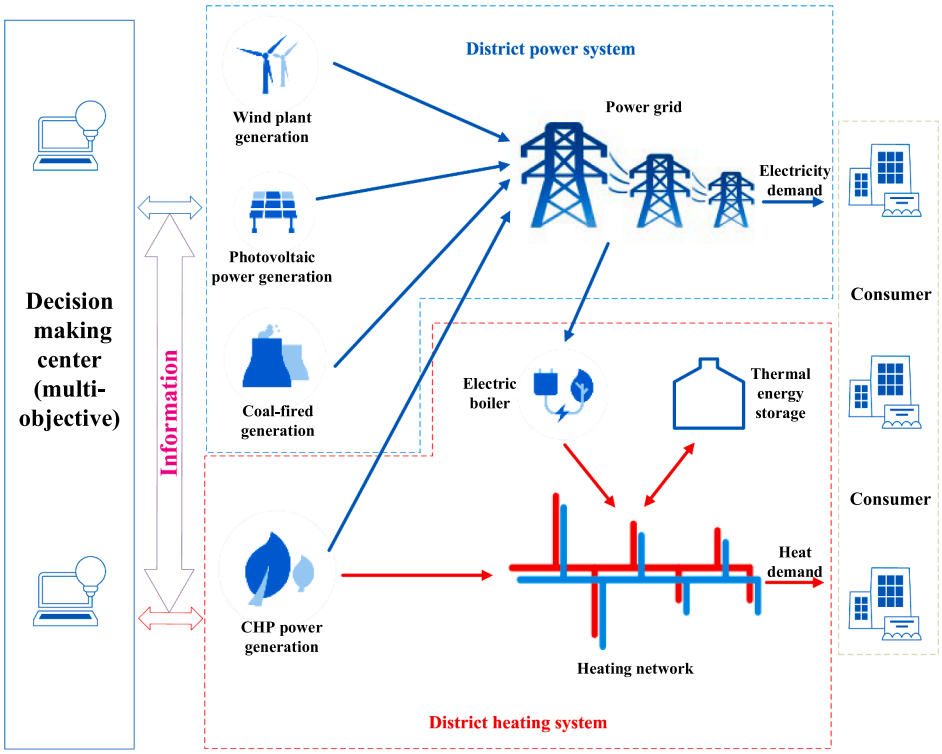

Fig. 1. A typical electro-thermal integrated energy system considered in this work.

where, P_{eb}^{t} is the power consumed by electric boiler, η_{eb} is the efficiency of electric boiler. The efficiency of electric boiler varies little during operation, therefore η_{eb} is a constant value.

(c) Thermal energy storage

Thermal energy storage is often used to compensate the imbalance between thermal supply and thermal demand.

$$Q_{tes}^{t+1} = Q_{tes}^{t} + H_{tes,char}^{t}\eta_{tes}^{char} - \frac{H_{tes,dis}^{t}}{\eta_{tes}^{dis}} \tag{6}$$

where, $H_{tes,char}^{t}$ and $H_{tes,dis}^{t}$ are the charge and discharge thermal power, η_{tes}^{char} and η_{tes}^{dis} are the charge and discharge efficiency. Q_{tes}^{t} is the heat storage amount at time t.

(d) Wind power generation

The generation of wind power can be expressed as a function of wind speed:

$$P_{WT}^{t} = \begin{cases} 0 v_t \le v_{in}, v_t \ge v_{out} \\ \dfrac{v_t - v_{in}}{v_r - v_{in}} P_{RWT} v_{in} \le v_t \le v_r \\ P_{RWT} v_r \le v_t \le v_{out} \end{cases} \tag{7}$$

where P_{WT}^{t} is the output power at time t, v_t is the wind speed at time t, v_{in} and v_{out} is the cut-in and cut-out wind speed respectively, v_r is the rated wind speed, P_{RWT} is the rated output power.

(e) Photovoltaic power generation

For photovoltaic, the output power depends on the installed capacity and the radiation intensity:

$$P_{PV}^{t} = f_{PV} P_{RPV} G_{T}^{t} / G_{T,STC} \tag{8}$$

where P_{PV}^{t} and G_{T}^{t} are the output power and radiation intensity at time t, respectively. f_{PV} is the derating factor, P_{RPV} is the rated output power and $G_{T,STC}$ is the radiation intensity corresponds to P_{RPV}.

2.2. Dynamic model of the heating network

(a) Hydraulic model of the heating network

1) Steady-state hydraulic model

The flow balance and loop pressure balance are considered in steady-state hydraulic model of hot water heating network [32]. The balances can be represented in matrix form:

$$\begin{cases} \boldsymbol{A_H m_{pipe}} = \boldsymbol{m_{node}} \\ \boldsymbol{B_f} \Delta H = 0 \\ \Delta H = K |\boldsymbol{m_{pipe}}| \boldsymbol{m_{pipe}} \end{cases} \tag{9}$$

where, $\boldsymbol{A_H}$ and $\boldsymbol{B_f}$ are the node-branch incidence matrix and the loop-branch matrix, respectively.$\boldsymbol{m_{pipe}}$ and $\boldsymbol{m_{node}}$ are the mass flow vectors in pipe and node separately.$|\boldsymbol{m_{pipe}}|$ represents the diagonal matrix of the absolute value of pipe mass flow. $\boldsymbol{K}$ is the pipe resistance vector.

2) Dynamic Hydraulic model

The hydraulic transients of heating network can be described by the quasilinear hyperbolic partial differential equations as follows.

Motion equation:

$$\frac{\partial H_{pipe}}{\partial x} + \frac{1}{g A_{pipe}} \frac{\partial Q_{pipe}}{\partial t} + \frac{f_{pipe}}{2 D_{pipe} A_{pipe}^{2}} |Q_{pipe}| Q_{pipe} = 0 \tag{10}$$

Continuity equation:

$$\frac{\partial H_{pipe}}{\partial x} + \frac{a^2}{g A_{pipe}} \frac{\partial Q_{pipe}}{\partial t} = 0 \tag{11}$$

where H_{pipe} is the piezometric head, a is the propagation velocity of water hammer wave, Q_{pipe} is the volume flow, f_{pipe} is the frictional resistance coefficient along the pipe. g is the gravitational acceleration, A_{pipe} is the cross-sectional area and D_{pipe} is the diameter.

(b) Dynamic thermal model of the heating network

According to thermodynamics, the thermal energy conservation equation can be expressed as [34]:

$$A_{pipe}\rho C_p \frac{\partial T_{pipe}}{\partial t} + C_p m_{pipe} \frac{\partial T_{pipe}}{\partial x} = A_{pipe}\lambda \frac{\partial^2 T_{pipe}}{\partial x^2} + \frac{1}{R}\left(T_a - T_{pipe}\right) \tag{12}$$

where T_{pipe} is the temperature of pipe,m_{pipe} is the mass flow rate in the pipe, R is the total thermal resistance. ρ, C_p and λ are the density, specific heat capacity and thermal conductivity of hot water, respectively. T_a is ambient temperature. For the district heating system (DHS), the heat conduction is relatively weak and can be neglected. Eq. (12) can then be written as:

$$A_{pipe}\rho C_p \frac{\partial T_{pipe}}{\partial t} + C_p m_{pipe} \frac{\partial T_{pipe}}{\partial x} = \frac{1}{R}\left(T_a - T_{pipe}\right) \tag{13}$$

(c) Node model

Nodes connect pipes to form a pipe network. If more than two inflow pipes connect node j, temperature mixing equation is applied to calculate the node temperature T_{node}^{j}.

$$T_{node}^{j} = \frac{1}{\sum_{i \in IN} m_{pipe}^{i}} \sum_{i \in IN} \left(m_{pipe}^{i} T_{pipe}^{i,end}\right) \tag{14}$$

where j refers to the node number, and $T_{pipe}^{i,end}$ is the temperature of pipe i for $i \in IN$ before mixing. Eq. (14) indicates that the temperature of node j is the weighted average value of the temperature of inflow pipes.

In addition to mixing nodes, there are also load nodes and heat source nodes in DHS, these nodes are modeled as the heat exchanger:

$$H_{node}^{j} = C_p m_{pipe}^{j} \left(T_{node}^{j,s} - T_{node}^{j,r}\right) \tag{15}$$

where H_{node}^{j} is the thermal power of node j, and the m_{pipe}^{j} is the mass flow of pipe, which is directly connected to node j. $T_{node}^{j,s}$ and $T_{node}^{j,r}$ are the supply and return temperature of node j.

2.3. The solution method

(a) **The solution method of Hydraulic model**

1) Newton-Raphson iterative method

Newton-Raphson iterative method is used to solve the steady-state hydraulic model of pipe network and obtain the mass flow distribution.

$$\boldsymbol{m}_{pipe}^{k+1} = \boldsymbol{m}_{pipe}^{k} - \boldsymbol{F}_{h}^{k} = \boldsymbol{m}_{pipe}^{k} - \left(\boldsymbol{J}_{h}^{-1} \Delta \boldsymbol{F}_{h}\right)^{k} \tag{16}$$

$$\boldsymbol{J}_h = \begin{bmatrix} \boldsymbol{A}_r \\ 2B|\boldsymbol{m}_{pipe}| \end{bmatrix} \tag{17}$$

$$\Delta \boldsymbol{F_h} = \begin{bmatrix} \boldsymbol{A}_r \boldsymbol{m}_{pipe} - \boldsymbol{m}_{node}^{r} \\ BK|\boldsymbol{m}_{pipe}|\boldsymbol{m}_{pipe} \end{bmatrix} \tag{18}$$

where k is the iterative times, $\boldsymbol{J}_h$ is the matrix in the hydraulic calculation and $\Delta \boldsymbol{F_h}$ is the mismatch vector. r represents the set of elements after removing the slack nodes (in the multi-heat-source heating network, a heat source node is usually selected as the slack node). $\boldsymbol{A}_r$ is the reduced node-branch matrix, $\boldsymbol{m}_{node}^{r}$ is the reduced node mass flow vector.

2) Characteristic line method

The characteristic line method is used to solve the dynamic hydraulic model which can transform Eq. (10) and Eq. (11) into ordinary differential equation.

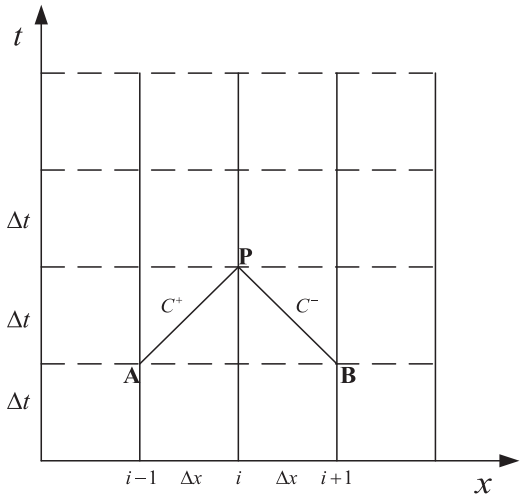

Fig. 2. Schematic diagram of characteristic line method.

$$C^{+}\begin{cases}\dfrac{g}{a}\dfrac{dH_{pipe}}{dt}+\dfrac{1}{A_{pipe}}\dfrac{dQ_{pipe}}{dt}+\dfrac{f_{pipe}}{2D_{pipe}{A_{pipe}}^{2}}|Q_{pipe}|Q_{pipe}=0\\ \dfrac{dx}{dt}=a\end{cases}\tag{19}$$

$$C^{-}\begin{cases}-\dfrac{g}{a}\dfrac{dH_{pipe}}{dt}+\dfrac{1}{A_{pipe}}\dfrac{dQ_{pipe}}{dt}+\dfrac{f_{pipe}}{2D_{pipe}{A_{pipe}}^{2}}|Q_{pipe}|Q_{pipe}=0\\ \dfrac{dx}{dt}=-a\end{cases}\tag{20}$$

C^{+} and C^{-} are two sets of compatibility equations, in which Eq. (19) and Eq. (20) are two characteristic lines on x-t plane as shown in Fig. 2.

We further divide one pipe into N sections, the length of each section is Δx, as shown in Fig. 2. The time step is Δt. When the H and Q values of $i-1$ and $i+1$ points are known, Eq. (19) and Eq. (20) are integrated along the characteristic line C, with the first-order approximation for the friction term, to obtain the finite difference equations:

$$C^{+}: H_{pipe}^{Pi}=C_P-BQ_{pipe}^{Pi}\tag{21}$$

$$C^{-}: H_{pipe}^{Pi}=C_M-BQ_{pipe}^{Pi}\tag{22}$$

where

$$C_P=H_{pipe}^{i-1}+BQ_{pipe}^{i-1}-RQ_{pipe}^{i-1}|Q_{pipe}^{i-1}|\tag{23}$$

$$C_M=H_{pipe}^{i+1}-BQ_{pipe}^{i+1}+RQ_{pipe}^{i+1}|Q_{pipe}^{i+1}|\tag{24}$$

$$B=\frac{a}{gA_{pipe}}\tag{25}$$

$$R=\frac{f\Delta x}{2gD_{pipe}{A_{pipe}}^{2}}\tag{26}$$

Q_{pipe}^{Pi} and H_{pipe}^{Pi} are the flow and piezometric head of the i^{th} pipe section at time t, respectively. Q_{pipe}^{i-1} and H_{pipe}^{i-1} are the flow and piezometric head of the i-1 pipe section at time $t-\Delta t$, respectively. Q_{pipe}^{i+1} and H_{pipe}^{i+1} are the flow and piezometric head of the $i+1$ pipe section at time $t+\Delta t$, respectively.

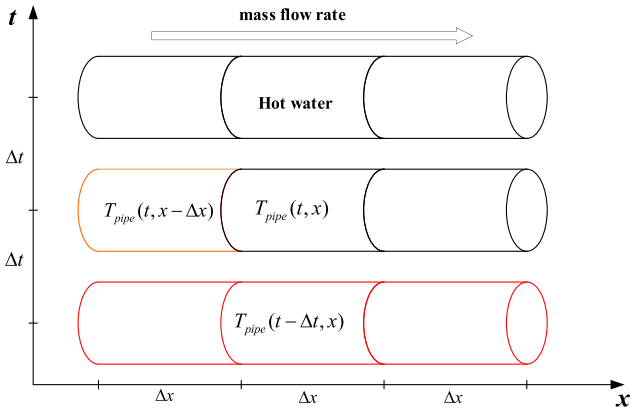

Fig. 3. Schematic diagram of solving pipeline temperature by upwind finite difference method.

In the above equations, when the H_{pipe} and Q_{pipe} values of each section of the pipe at $t=0$ are known, the values of H_{pipe} and Q_{pipe} can be obtained by using the above equations at any internal grid node.

Boundary condition:

Speed-control Pump: The characteristics of a normal working pump can be determined by its characteristic curve, which can be written as:

$$H_{pump}^{in}-H_{pump}^{out}=H_s+\varphi_1Q_{pump}^{in}+\varphi_2{Q_{pump}^{in}}^{2}\tag{27}$$

where φ_1 and φ_2 are coefficients representing the pump characteristic curve. H_{pump}^{in} and H_{pump}^{out} are the piezometric heads at the inlet and outlet of the pump.

$$Q_{pump}^{in}=\frac{B_{in}+B_{out}-\varphi_1}{2\varphi_2}\left(1-\sqrt{1-\frac{4\varphi_2(H_s-C_P-C_M)}{(B_{in}+B_{out}-\varphi_2)^{2}}}\right)\tag{28}$$

More discussions about boundary conditions can be found in [35].

(b) The solution method of thermal model

Eq. (13) is a partial differential equation, which can be solved by implicit upwind method Fig. 3. Comparing with the explicit method, the implicit upwind method has a faster calculation speed, higher orders of accuracy and no criterion for numerical stability. According to [34], Eq. (13) can be written as:

$$A_{pipe}\rho C_p\frac{T_{pipe}(t,x)-T_{pipe}(t-\Delta t,x)}{\Delta t}+C_pm_{pipe}\frac{T_{pipe}(t,x)-T_{pipe}(t,x-\Delta x)}{\Delta x}=\frac{1}{R}\left(T_a-T_{pipe}(t,x)\right)\tag{29}$$

$$T_{pipe}(t,x)=\left(T_{pipe}(t-\Delta t,x)+\frac{\mu(t)\Delta t}{\Delta x}T_{pipe}(t,x-\Delta x)+\frac{\Delta t}{A_{pipe}\rho C_pR}T_a\right)/\left(1+\frac{\mu(t)\Delta t}{\Delta x}+\frac{\Delta t}{A_{pipe}\rho C_pR}\right)\tag{30}$$

where, $\mu(t)=m_{pipe}/(A_{pipe}\rho)$, which is the flow velocity. Eq. (30) indicates that the temperature at time t and segment x can be calculated from the temperature at the previous time and position. At time t, the

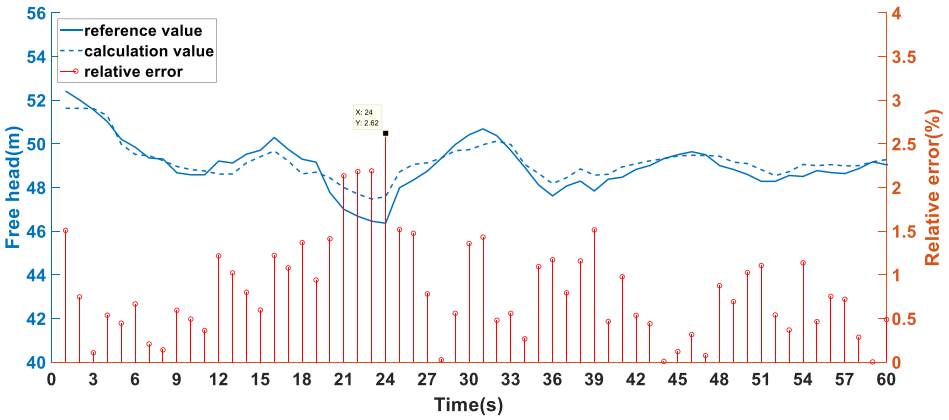

Fig. 4. Our calculated results, measured data in [35] and the corresponding relative errors of the free head (pressure) in the heating network.

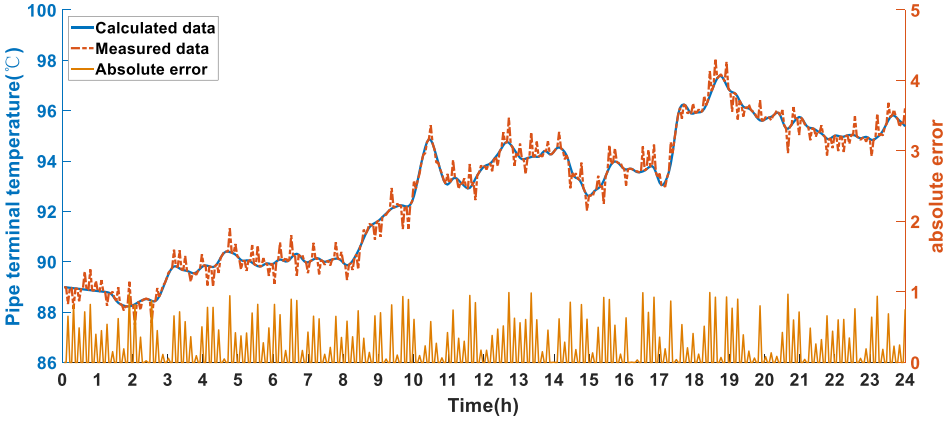

Fig. 5. Our simulated results, the measured data in [34] and the corresponding absolute errors of pipe terminal temperature in the heating network.

mass flow rate m_{pipe},$T_{pipe}(t-\Delta t,x)$and$T_{pipe}(t,x-\Delta x)$ are known, since they are the values of the previous time point and the previous position, respectively. The boundary condition at pipe inlet is $T_{pipe}(t,x=0)=T_{in}(t)$.

2.4. Validation of the thermal and hydraulic models of the heating network

A case in [35] is introduced to verify the proposed hydraulic transient model. The pipe network system consists of 19 pipelines and 12 nodes, which is supplied by two high-level reservoirs, and the total hot water flowrate of the system is 0.29 m^3/s. Our calculated results, the measured data in [35] and the corresponding absolute error are shown in Fig. 4. The maximum absolute error is 1.2145 m and the maximum relative error is 2.62%. Therefore, our proposed model is trustful and can accurately model the hydraulic transient characteristics of real heating network system.

To validate our proposed thermal dynamic model of the heating network, the measured data from Shijiazhuang Luhua CHP plant [34] is chosen to compare. Luhua CHP plant is connected to the heat exchange station through a 9.25 km pipeline. The calculated results from the proposed thermal dynamic model, the measured data from [34] and the corresponding absolute error are shown in Fig. 5. The average absolute error is 0.1647 ℃ and the maximum absolute error is 0.9910 ℃. Therefore, the proposed model is able to model the thermal dynamic characteristics of the real heating network system accurately.

3. Bi-level multi-objective optimization

The bi-level structure can effectively decompose the complex problem into two relatively simple sub-problems, and then solve the two sub-problems separately, which can improve the solution accuracy.

3.1. The structure of bi-level multi-objective optimization

The bi-level optimization scheduling model attempts to search the best solution in the respective search space. The optimization interval is one hour, and the optimization time frame is one day (24 h).

For the district heating system (DHS), the optimization variables are: the thermal power outputs from the CHP and the electric boiler, the charge and discharge thermal power of thermal energy storage and the thermal power contained in heating network. For the district power system (DPS), the optimization variables are the electric power outputs from the CHP, the coal-fired units, the renewable power systems (wind farm and photovoltaic) and the power consumed by the electric boiler.

3.2. Outer layer model: economic-environmental assessment model for the IES

Objective functions

To achieve the goal of assessing the economic-environmental equilibrium strategy, the outer layer objectives are to minimize the total operation cost and the total carbon emission.

Objective 1: minimizing the total operation cost

The total operation cost includes the fuel cost of CHP unit and the operation cost of all devices. It can be formulated as follows:

$$C_{fuel} = \sum_{t=1}^{T} p_{gas} V_{gas}^{t} \tag{31}$$

$$C_{operation} = \sum_{t=1}^{T} \left(c_{coal} P_{coal}^{t} + c_{chp} P_{chp}^{t} + c_{wt} P_{wt}^{t} + c_{pv} P_{pv}^{t} + c_{eb} H_{eb}^{t} + c_{tes} H_{tes}^{t} \right) \tag{32}$$

$$minf_1 = C_{fuel} + C_{operation} \tag{33}$$

where p_{gas} is the price of natural gas per unit volume, V_{gas}^{t} is the natural gas volume consumed by CHP, $c_{coal}, c_{chp}, c_{wt}, c_{pv}, c_{eb}, c_{tes}$ are the unit operation cost of coal-fired power plant, CHP, wind turbine, photovoltaic, electric boiler and thermal energy storage, respectively.

Objective 2: minimizing the total carbon emission

The main sources of carbon emission are coal-fired power plants and CHP. The carbon intensity coefficients α_1, α_2, α_3, β_1, β_2, and β_3 are introduced in the model to estimate the total carbon emission:

$$Carbon_{chp} = \sum_{i=1}^{T} \left(\alpha_1 + \alpha_2 P_{chp}^{t} + \alpha_3 \left(P_{chp}^{t} \right)^2 \right) \tag{34}$$

$$Carbon_{coal} = \sum_{i=1}^{T} \left(\beta_1 + \beta_2 P_{coal}^{t} + \beta_3 \left(P_{coal}^{t} \right)^2 \right) \tag{35}$$

$$minf_2 = Carbon_{chp} + Carbon_{coal} \tag{36}$$

Constraints of the outer layer model

The DHS is selected as the outer layer system. The constraints of the outer layer system contain energy flow balance, devices operational constraints and heating network operational constraints.

(1) Thermal energy flow balance

The thermal energy flow balance in DHS (including the heating network) should consider the thermal power transmission loss. The output of CHP, EB and TES is equal to the thermal load demand plus the transmission loss in pipelines:

$$H_{chp}^{t} + H_{eb}^{t} + H_{tes,dis}^{t} - H_{tes,char}^{t} = H_{load}^{t} + H_{loss}^{t} \tag{37}$$

where H_{chp}^{t},H_{eb}^{t} are the thermal power output of CHP and EB, respectively. $H_{tes,dis}^{t}$,$H_{tes,char}^{t}$ are the discharge and charge thermal power of TES, respectively. H_{load}^{t},H_{loss}^{t} are the thermal load demand and the transmission loss in pipelines, respectively.

(2) Operational constraints of heating devices

CHP unit:

The relationship between thermal power and electrical power is formulated in Eq. (1)-(4). The electrical power P_{chp}^{t} is selected as the constraint objective,

$$P_{chp}^{min} \le P_{chp}^{t} \le P_{chp}^{max} \tag{38}$$

where P_{chp}^{min} and P_{chp}^{max} are the minimum and maximum power output of CHP, respectively.

If the power output of the equipment changes fast over a threshold value in a certain time interval, the unit will have safety issues. It is necessary to restrict the ramping rate of units.

$$-R_{chp}^{down} \le P_{chp}^{t} - P_{chp}^{t-1} \le R_{chp}^{up} \tag{39}$$

where R_{chp}^{down} and R_{chp}^{up} are the down and up ramping limits, respectively.

Electric boiler:

The operation constraints and ramping limits of electrical boiler are:

$$H_{eb}^{min} \le H_{eb}^{t} \le H_{eb}^{max} \tag{40}$$

$$-R_{eb}^{down} \le H_{eb}^{t} - H_{eb}^{t-1} \le R_{eb}^{up} \tag{41}$$

where H_{eb}^{min} and H_{eb}^{max} are the minimum and maximum output thermal power of EB, respectively. R_{eb}^{down} and R_{eb}^{up} are the down and up ramping limits, respectively.

Thermal energy storage:

To ensure a sustainable and stable operation of the thermal energy storage unit, the charge and discharge amount must be controlled. Meanwhile, it is assumed that the charge and discharge status will not occur simultaneously, so auxiliary binary variables b_{char}^{t} and b_{dis}^{t} are introduced to indicate this status:

$$0 \le H_{tes,char}^{t} \le b_{char}^{t} H_{tes,char}^{max} \tag{42}$$

$$0 \le H_{tes,dis}^{t} \le b_{dis}^{t} H_{tes,dis}^{max} \tag{43}$$

$$0 \le b_{char}^{t} + b_{dis}^{t} \le 1, b_{char}^{t}, b_{dis}^{t} \in \{0,1\} \tag{44}$$

where $H_{tes,char}^{max}$ and $H_{tes,dis}^{max}$ are the maximum charge and discharge thermal power of TES, respectively.

3.3. Inner layer model: optimal economic operation model for power system

The CHP output power P_{chp}^{t} and the output of other heat source calculated through the outer layer are transferred to the inner layer as boundary conditions. The inner layer model aims to gain the optimal operation strategy under the above boundary conditions, and the results calculated through the inner layer of P_{coal}^{t}, P_{wt}^{t}, P_{pv}^{t}, H_{eb}^{t} and H_{tes}^{t} are transferred back to the outer layer for overall evaluation. The inner layer takes the economy as the objective function.

$$minf_3 = \sum_{t=1}^{T} \left(c_{coal} P_{coal}^{t} + c_{wt} P_{wt}^{t} + c_{pv} P_{pv}^{t} + c_{eb} H_{eb}^{t} + c_{tes} H_{tes}^{t} \right) \tag{45}$$

Constraints of inner layer

The DPS is selected as the inner layer system. The constraints of the inner layer system contain power flow balance and device operational constraints. For simplicity, the values of electricity transmission losses are neglected, and only the transmission line capacity constraint is considered. Electrical power generated by CHP, wind farm, photovoltaic plant and coal-fired plant should meet the load demand, and ensure the normal operation of electric boiler.

(1) Electrical energy flow balance

$$P_{chp}^{t} + P_{wt}^{t} + P_{pv}^{t} + P_{coal}^{t} - P_{eb}^{t} = P_{load}^{t} \tag{46}$$

where P_{load}^{t} is the electrical load demand.

(2) Operation constraints of power supply devices

CHP unit:

CHP is an electrothermal coupling equipment, which can generate electricity and heat at the same time. The constraints about CHP are defined in Eqs. (38)–(39).

Wind plant and Photovoltaic plant:

Generating power from wind and photovoltaic plants is beneficial for conserving energy and reducing emission. But the output is influenced by local wind and radiation resources. The actual power generation is constrained by the power forecast.

$$0 \le P_{wt}^{t} \le P_{wt,forecast}^{t} \tag{47}$$

$$0 \le P_{pv}^{t} \le P_{pv,forecast}^{t} \tag{48}$$

where $P_{wt,forecast}^{t}$ and $P_{pv,forecast}^{t}$ are the power forecast on each time step t, which are assumed to be known. The difference between the actual output and the forecast output is the amount of wind and photovoltaic power curtailment.

Coal-fired power generation units:

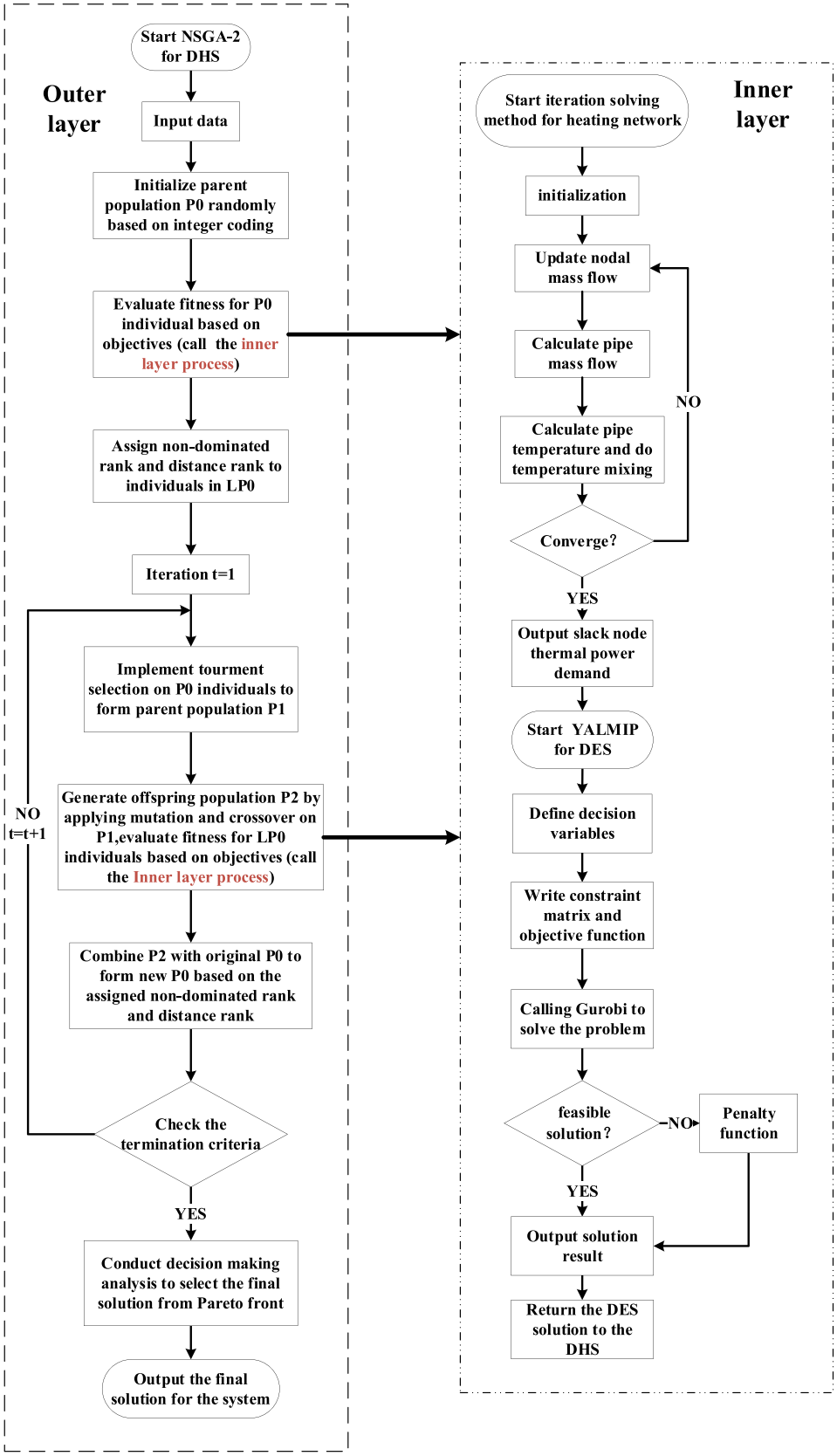

Fig. 6. Flow chart of solving the bi-level multi-objective optimization.

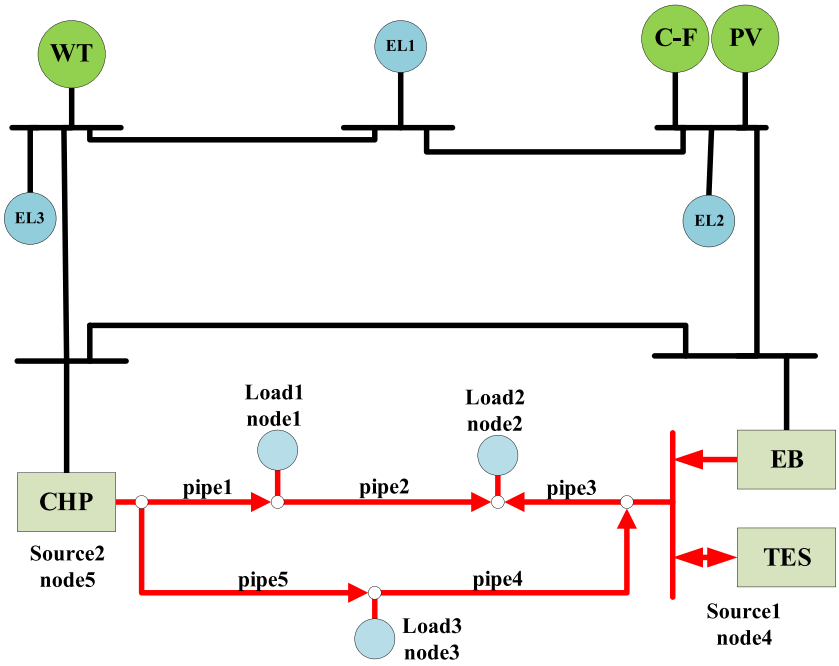

Fig. 7. Structure diagram of IES.

Similar to the CHP unit, the operation of coal-fired unit is limited by the rated capacity, as well as the ramping constraint:

$$0 \le P^{t}_{coal} \le P^{max}_{coal} \tag{49}$$

$$P^{t}_{coal} - P^{t-1}_{coal} \le x_t R^{up}_{coal} + (1 - x_t) R^{down}_{coal} \tag{50}$$

where P^{t}_{coal} is the output power of the coal-fired unit at time step t. P^{max}_{coal} is the maximum output power of coal-fired unit. R^{up}_{coal}, R^{down}_{coal} are the up and down ramping limit, respectively. x_t is the state variable where $x_t \in \{0,1\}$.

Power transmission constraint:

The transmission power is limited by the rated transmission line capacity:

$$0 \le P^{t}_{line} \le P^{max}_{line} \tag{51}$$

where P^{t}_{line} is the transmitted power in transmission lines at time step t, and P^{max}_{line} is the rated transmission line capacity.

3.4. Solution method

In this work, the optimization model is a mixed integer nonlinear programming (MINLP) model. The nonlinear part is the CHP variable efficiency model, the heating network transient model and the carbon emission objective function. Heuristic algorithm is advantageous in solving this kind of nonlinear problems. NSGA-II algorithm, a fast non-dominated multi-objective optimization algorithm with elite retention strategy, is a multi-objective optimization algorithm based on Pareto optimal solution. However, heuristic optimization producers are experience-based techniques defined as a quick method for obtaining solutions for optimization problems, in which optimal solutions are not achievable using mathematical methods in finite time [37,38]. As just describe, due to the randomness of heuristic algorithm, it cannot guarantee to obtain the optimal solution. On the contrary, the deterministic algorithm is more accurate but time consuming because it needs to linearize the nonlinear items before solving. Therefore, the NSGA-II algorithm is combined with the deterministic algorithm solver Gurobi to obtain the Pareto solution set efficiently and accurately.

1. NSGA-II for the outer layer

The optimization problem of the outer layer is a nonlinear multi-objective programming. Therefore, the integer coding NSGA-II is used to solve the outer layer multi-objective optimization. As a thermoelectric coupling equipment, the electricity output of CHP will affect both the power system and the thermal system. Therefore, CHP power output is selected as the decision variable in the outer layer optimization. Meanwhile, more variables can be solved by the inner layer to obtain a higher accuracy.

As shown in Fig. 6, the solution process can be summarized as follows:

1. Select the power output of CHP unit (P^{t}_{chp}) as the decision variable. The initial population P_0 is initialized randomly. P_0 is then transferred to the inner layer to obtain the corresponding optimal solution, namely, the optimal scheduling strategy. The rank value of each individual is initialized.
2. Set $t = 0$, the individuals are selected from P_0 by binary tournament method and being crossed and mutated to produce a new generation of population P_1.
3. The objective value of P_1 is calculated similarly as step 1. The value of fitness function is evaluated by both the outer and the inner layers.
4. By combining P_0 and P_1, the combined population P_2 is produced.
5. Then P_2 is sorted by non-dominance, and the strategies of crowding out and elitism retention are implemented. N individuals were selected to form a new generation population P_t.
6. Set $t = t + 1$, return to step 3 and iterate until the end condition is met.

Table 4
Parameters of heating network [32].

Pipe number	Diameter (mm)	Length (m)	Thermal conducive coefficient
1	500	1000	0.125
2	300	800	0.125
3	500	1000	0.125
4	400	1000	0.125
5	400	1000	0.125

Pseudo code

while condition:
  $P_2 = P_0 + P_1$
  $F = fast\_nondominate\_sort(P_2)$
  $P_{0+t} = []$
  $i = 0$
  $while len(P_{0+t}) + len(F[i]) < N:$
    $crowding\_distance\_assignment(F[i])$
    $P_{0+t} += F[i]$
    $i += 1$
    $P_{0+t} += F[i][0 : N - len(P_{0+t})]$
    $P_{1+t} = make\_new\_generation(P_{0+t})$
    $t = t + 1$

2. Iterative solution for the dynamic heating network model

It is assumed that the mass flow distribution in the pipe network remains unchanged during the one step thermal transient calculation. Thermal transient process can be calculated by Eq. (30).

After using Eq. (16) and Eq. (30) for calculation, the mass flow at each node is obtained. The convergence is determined by comparing the node flow with calculations from the previous time step:

$$max\left|\frac{m_{node}^{k+1} - m_{node}^{k}}{m_{node}^{k}}\right| \le \varepsilon \tag{50}$$

where ε is the preset tolerance value.

When using the quantity regulation method, the temperature at the heat source is set as constant, and one heat source node is selected as the slack node. By adjusting the mass flow of other source nodes, the demand of heat load can be met, and the heat power supply at the slack node can be obtained.

3. Gurobi for the inner layer

The calculation results of the outer layer, including the CHP output in NSGA-II and the thermal power of the slack node calculated by the heat supply network, are transferred to the inner layer. Then Gurobi is called to solve the inner layer model based on YALMIP. If a feasible solution is not available, the penalty function will be called to discipline the output value. Finally, the optimization results are exported to the outer layer.

4. Case study

4.1. Introduction of the prototype system

To verify the effectiveness of the proposed bi-level optimization model, a 5-node power system with 5-node thermal system are designed. The thermal load of this test system is provided by CHP, electric boiler and thermal energy storage. The district power system includes wind

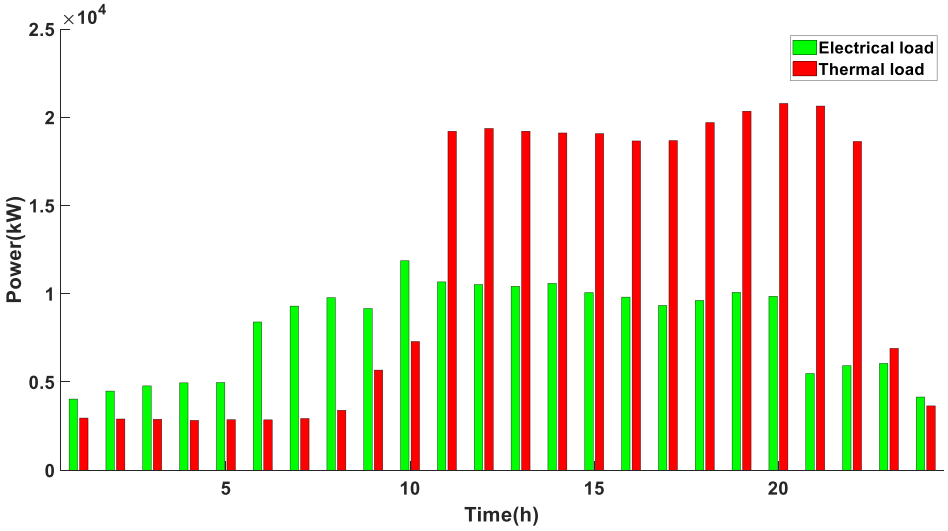

Fig. 8. Electricity and heat load demand of a typical winter day.

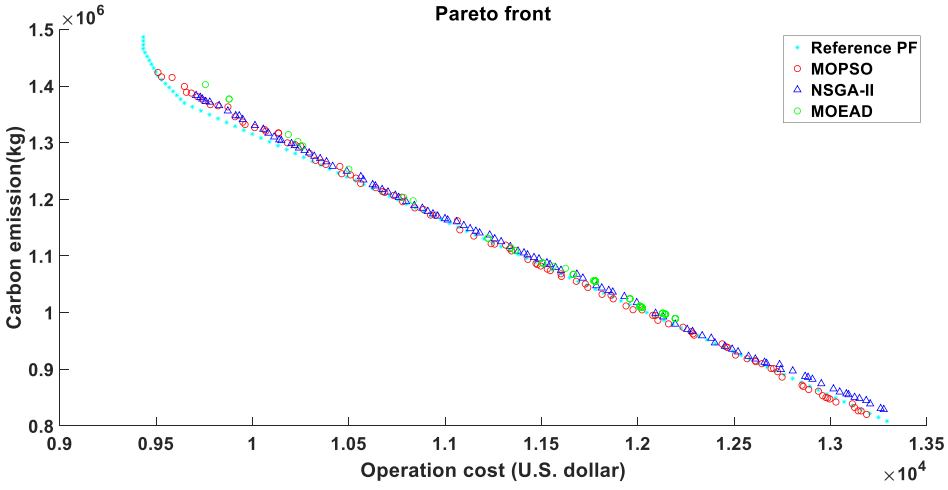

Fig. 9. Pareto optimal front of system operation cost (U.S. dollar) and carbon emission for different solution methods.

Table 5
Performance comparison of various algorithms.

Index	method	Best	Worst	Average
Computation Time (s)	**NSGA-II**	**579.52**	**663.49**	**610.12**
	MOPSO	1004.57	1100.47	1044.80
	MOEA/D	1007.88	1088.68	1059.28
Hypervolume	**NSGA-II**	**2.0057**	**1.9987**	**2.0022**
	MOPSO	1.9887	1.9801	1.9827
	MOEA/D	1.9801	1.9711	1.9782

plant, photovoltaic plant, coal-fired plant and power grid; The district heating system includes CHP, electric boiler, thermal energy storage and district heating network. The structure of the prototype system is illustrated in Fig. 7. The parameters of devices are shown in Table 3, and parameters of pipelines are shown in Table 4.

The system contains 3 electricity load nodes and 3 heat load nodes. The optimization interval is 1 h and a typical winter day with strong electrothermal coupling is selected as the period of case study. The load profile is shown in Fig. 8. The load distribution ratio of the electric load node is 1:1:1, while the ratio of thermal load node is 3:3:4.

The natural gas consumed by CHP is obtained from gas market in the price of 0.323 U.S. dollar/m^3. The electric power consumed by the electric boiler is directly obtained from the DPS. Since the electric boiler has high efficiency and little change in the actual allowable process, a constant efficiency of 0.88 is adopted. Similarly, the charge and discharge efficiency are set to be 0.9. In DHS, the temperature of the heating sources is set to be 80℃, while the return temperature in the heating loads is set to be 50℃.

4.2. Results and discussions

1. Algorithm verification

The proposed optimization model solved using NSGA-II & Gurobi, MOPSO & Gurobi, and MOEA/D & Gurobi are compared to demonstrate the advantages of the proposed solution method. Gurobi based on ε −constraintmethod[36] is adopted as a reference Pareto front to verify the effectiveness of the proposed solution method. All calculations are completed on a computer with 8 GB RAM and Intel Core i5-104000 CPU @ 2.90 GHz.

Several experiments are conducted to obtain the best parameters of heuristic algorithm. For NSGA-II, the population size is 100, and the maximum generation is 50. For MOPSO, the population size is 200, the repository size is 100, and the maximum generation is 50. For ε −constraintmethod, the number of evaluations is 100.

The Pareto fronts of four solution methods for the test system are graphically presented in Fig. 9. The longest profile composed of sky-blue plum blossom is the Pareto front with the ε −constraintmethod in Gurobi which linearizes the constraints. The solution sets obtained by MOPSO, MOEAD and NSGA-II, which adopt the nonlinear constraints to ensure the accuracy of scheduling, are all near the reference line. It shows that the optimization method designed in this work is practical and generic.

The computation time for various heuristic algorithms to iterate 50 rounds are compared in Table 5. NSGA-II is nearly 40% faster than the other two methods. The hypervolume is also introduced here to evaluate the performance of various algorithms. The A higher hypervolume value indicates more comprehensive performance of the algorithm. NSGA-II has the highest hypervolume value than the others. In summary, NSGA-II can get the Pareto solution set faster and better, which has the best comprehensive performance.

In Fig. 10, the optimal Pareto front of the proposed optimization method is obtained for the typical winter day. Fuzzy satisfying method is adopted to selected the best solution among the obtained optimal Pareto front [36]. The blue star in Fig. 10 represents the selected solution, with operation cost of 10,150.18 U.S. dollars and carbon emission of 1303.7 tons.

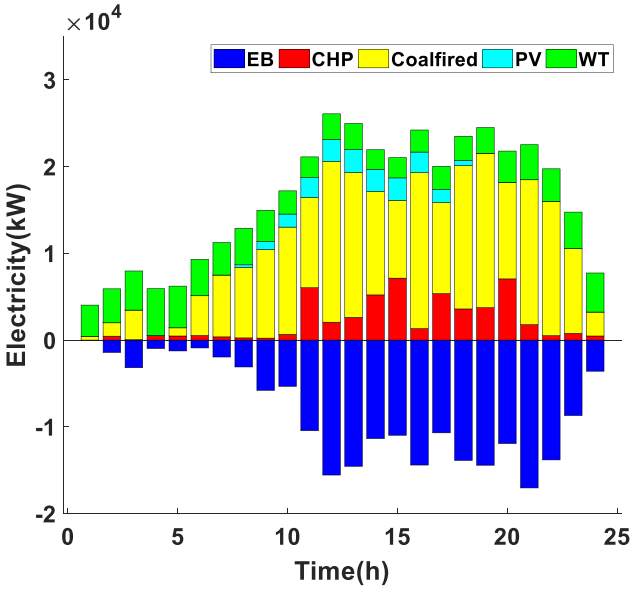

Fig. 11. Hourly electricity scheduling strategy.

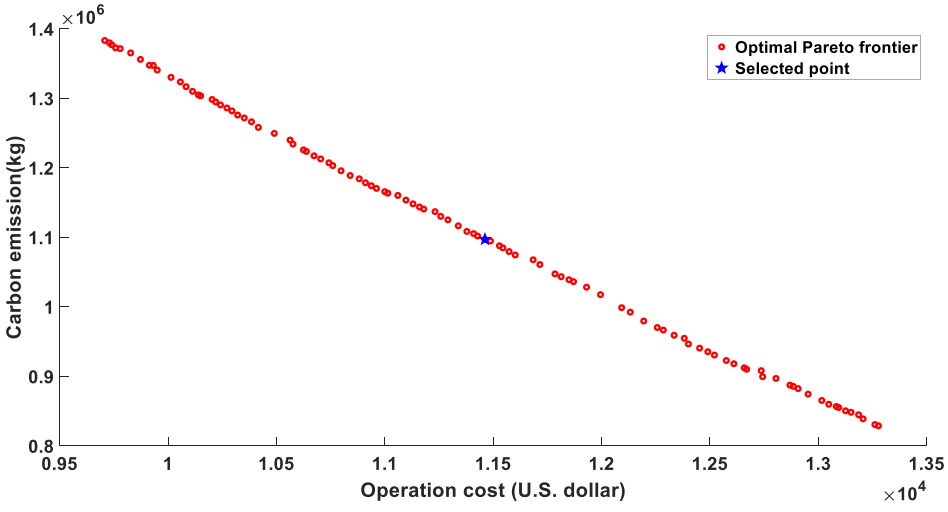

Fig. 10. Optimal Pareto front for the proposed method and the selected solution.

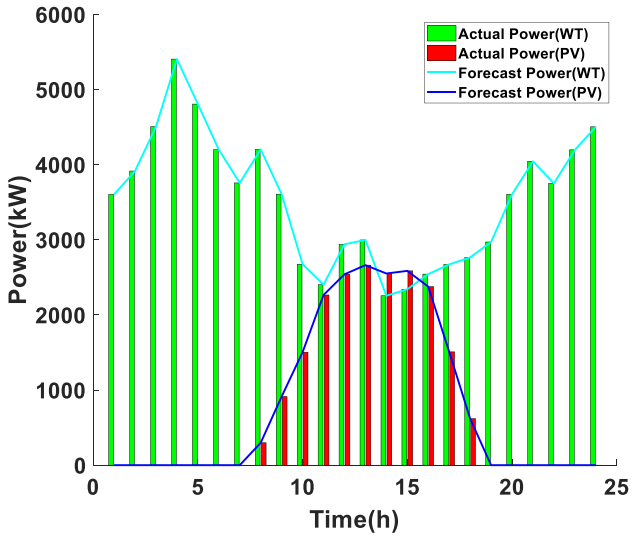

Fig. 12. The actual and forecasted power output from the wind and photovoltaic plants. (The proposed method).

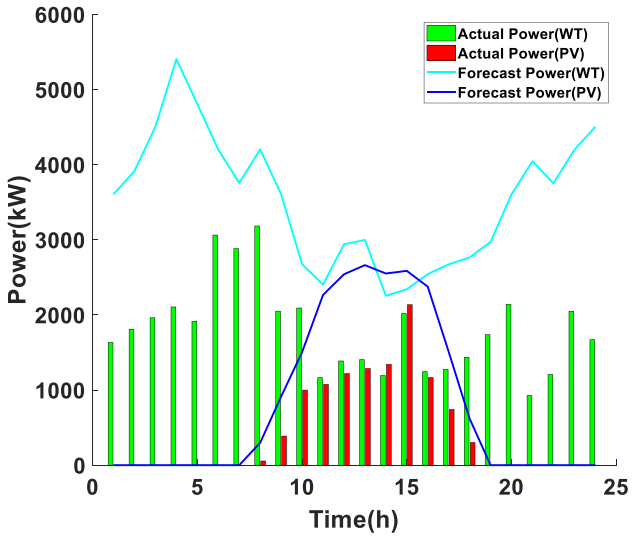

Fig. 14. The actual and forecasted power output from the wind and photovoltaic plants (the benchmark method).

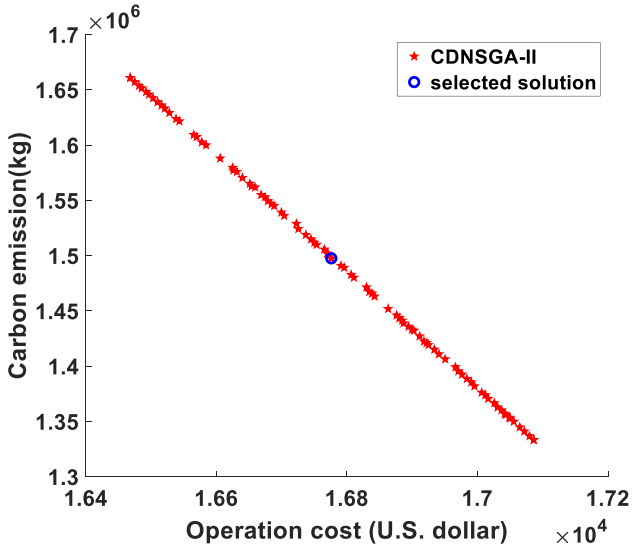

Fig. 13. Optimal Pareto front of the benchmark method and the selected solution.

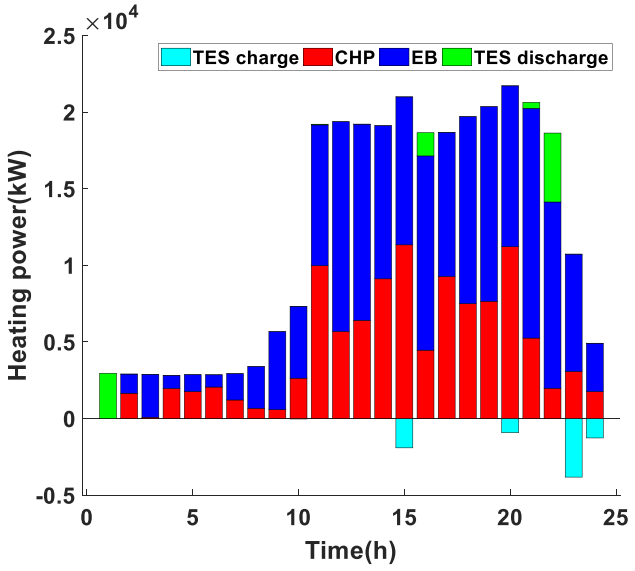

Fig. 15. Hourly heating scheduling strategy.

2. Comparison of scheduling strategies

(a) District power system

The optimized scheduling strategies of DPS under the optimal condition are shown in Fig. 11. In addition to the electricity load, electrical boiler also consumes a lot of electricity in the IES. The major part of electricity load in the DPS is provided by the coal-fired plant. Because of the limited capacity and high operation cost, CHP is the other main provider. As shown in Fig. 12, the utilization rate of clean and cost-effective wind power and photovoltaic is 100%.

In order to demonstrate the benefits of the proposed optimization method, a benchmark method is introduced: a monolayer model that is solved by NSGA-II based on constraint domination (CDNSGA-II). For CDNSGA-II, the population size is 100, and the maximum generation is 1000. The optimization result is shown in Fig. 13 and the utilized renewable power is shown in Fig. 14. In the selected optimization point, the operation cost is 16776.01 U.S. dollars, the carbon emission is 1497.6 tons and the utilization rate of renewable power is 46.736%.

The comparison between the above two methods shows that the proposed method can provide more economical and environmentally friendly scheduling advices for decision-makers by greatly improving the utilization rate of wind and photovoltaic.

(b) District heating system

The optimized scheduling strategies of DHS are shown in Fig. 15. The heating scheduling strategy shows that the heat load is mainly provided by CHP and EB, while TES only plays an auxiliary role.

The mass flow distribution in pipe network is shown in Fig. 16, corresponding to the thermal output from the two heat sources. And some regular patterns are hidden in the mass flow changes, Pipe 1 and Pipe 5 have the similar change pattern. It is because that Pipe 1 and Pipe 5 are connected to the same heat source node. Similarly, Pipe 3 and Pipe 4 also have the same characteristics. Meanwhile, the mass flow variation of Pipe 4 and Pipe 5 have obvious complementary characteristics since they are connected to the same heat load node. Pipe 3 and Pipe 2 also have the same characteristics.

The temperature changes within the pipe network are shown in Fig. 17 and Fig. 18. Results show that Pipe 1 and Pipe 5 have little temperature variation. The reason is that the mass flow in Pipe 1 and Pipe 5 are higher than that of others. The temperature varies greatly in

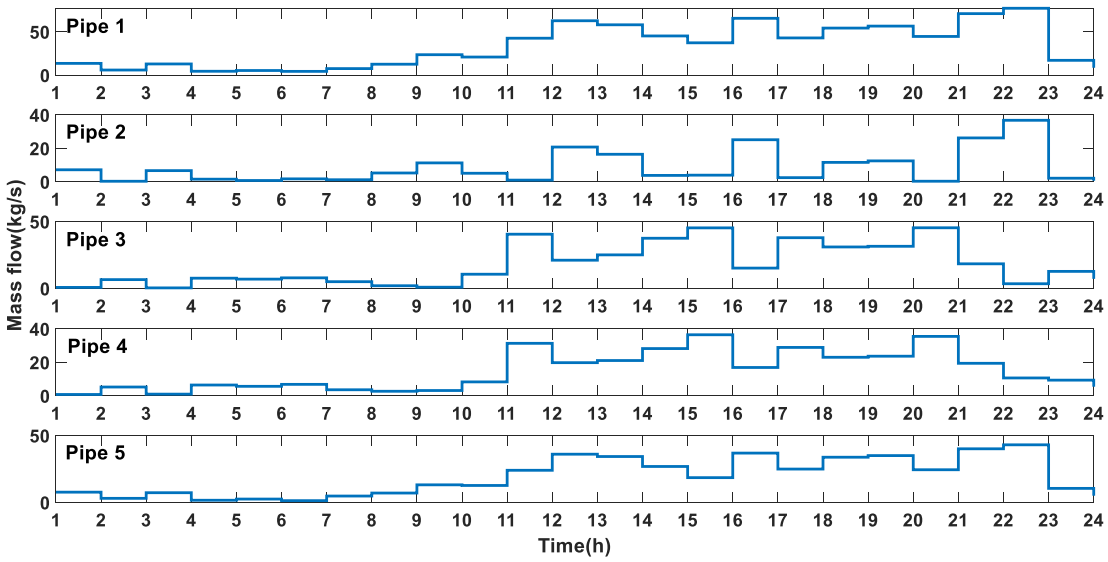

Fig. 16. Mass flow changes in each pipe.

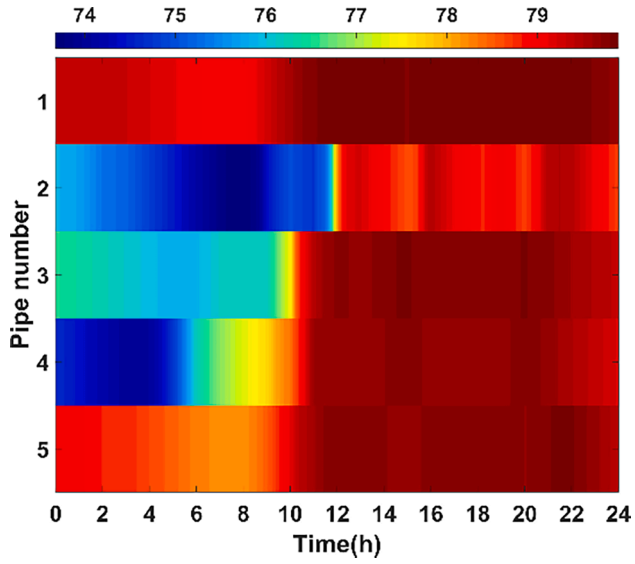

Fig. 17. Temperature change in each pipe.

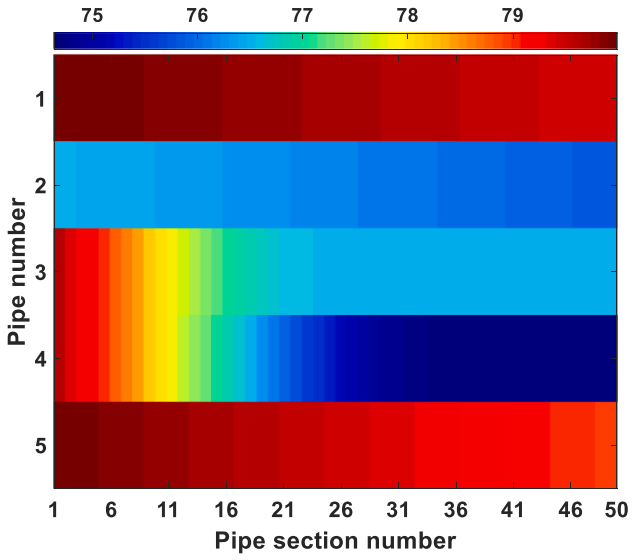

Fig. 18. Temperature distribution of each pipe at time 2.

Pipe 2 and Pipe 4. At the beginning of scheduling, the mass flow of Pipe 2, Pipe 3 and Pipe 4 is small, and the mass flow is close to 0 at some times, so the temperature of this period is low. With the increasing load demand, the mass flow of pipe network increases, and the temperature also increases. As Pipe 2 is located in the center of heating network, its mass flow is always smaller than that of others, so its temperature is also lower (with the lowest temperature of 73.7 ℃). It can also be seen that inertia is presented when the temperature changes with the mass flow.

The detailed temperature variation with mass flow is shown in Fig. 19. For all pipes, the temperature decreases from 0 h to 8 h, due to the small mass flow in this period. Meanwhile, the pipe temperature is more sensitive to the change of mass flow in the low mass flow operation stage. At 12 h, the temperature of each pipe reaches the highest value, and then the temperature fluctuates slightly. Even at 23 h to 24 h, the mass flow drops to the same level as that at 0 h to 6 h, the temperature doesn't drop to the same level, which reflects the heat transmission inertia in the heating network. Pipe 1 and Pipe 5 have the same mass flow variation profile but different magnitude. Since the mass flow in Pipe 1 is approximately twice of Pipe 5, the minimum and maximum temperature of Pipe 1 are higher than that of Pipe 5. Since the inlet of Pipe 2 is connected with the outlet of Pipe 1 and Load 1, the temperature and the mass flow of Pipe 2 are both lower than that of other pipes.

In this work, quantity regulation mechanism is adopted in the DHS, which controls the mass flow in the pipe network through the valves at the heat exchange station. It is assumed that the valve operation time is consistent with the scheduling time, and the response time of valves is negligible. The mass flow of nodes obtained in Section 3 is input into the hydraulic transient analysis. During the scheduling period, a total of 23 mass flow changes occurred, i.e. Step = 1 to 23. The hydraulic transients of each step are shown in Fig. 20. Combined with the results of the mass flow change, the pressure variation in the pipe has the opposite trend with the mass flow change. Pipe 4 and Pipe 5 have the same pressure variation of each stage, since Pipe 4 and Pipe 5 are connected to the same load node. Similarly, Pipe 2 and Pipe 3 also have the same characteristics. From Step 1 to Step 7, the pressure change of each pipe is not dramatic, since the change of mass flow in this period is not large. In Step 8 to Step 12, the pressure of each pipe changes dramatically. At this stage, the demand of heat load begins to ramp up rapidly, which leads to the dramatic change of mass flow and pressure in the pipe network.

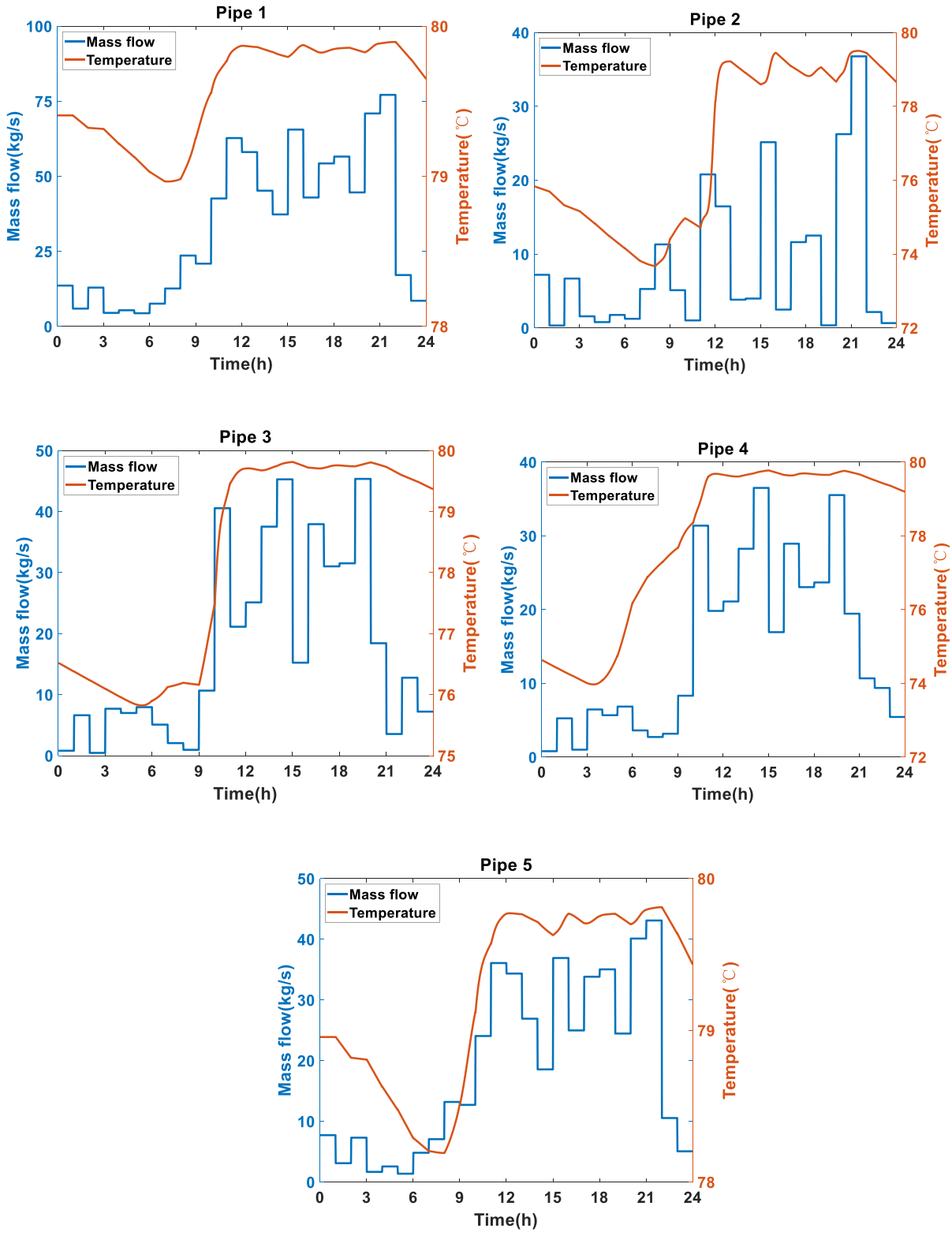

Fig. 19. Mass flow variation and temperature response of each pipe.

From Step 13 to Step 20, the pressure changes of each pipe return to stable conditions, although the mass flow of the pipe network in this stage is large. From Step 21 to Step 23, the pressure of each pipe changes dramatically again, while the demand of heat load drops rapidly and the flow rate begins to decrease.

According to Fig. 20, the scheduling strategy proposed in this work is appropriate to ensure safe operation of the pipe network. If the hydraulic analysis finds that the pressure change caused by quantity regulation exceeds the tolerance of the pipeline, it is feasible to control the mass flow change rate to prevent strong transient hydraulic flow when the load demand changes strongly.

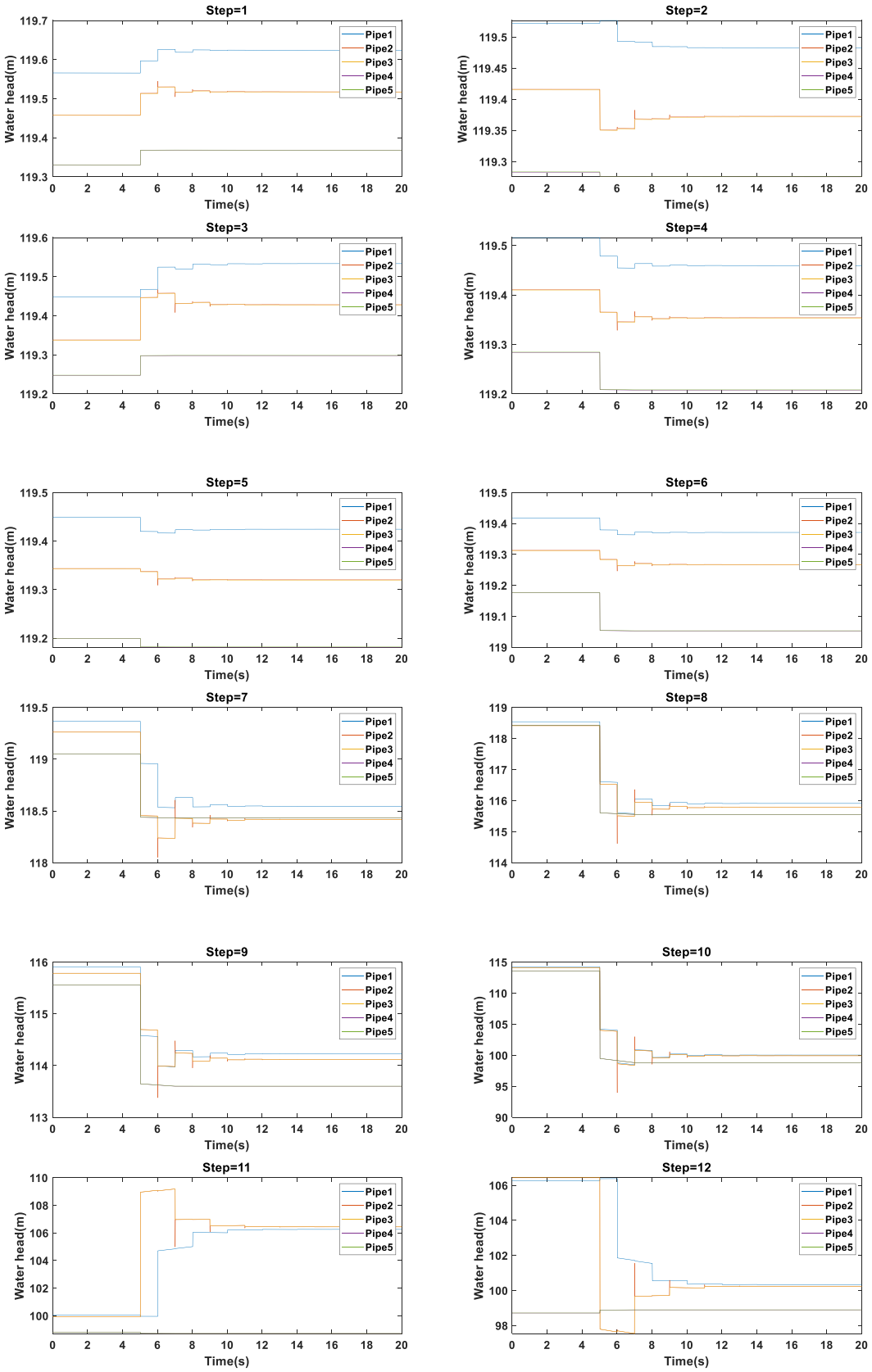

Fig. 20. Hydraulic transient changes in different operation stages of the pipeline.

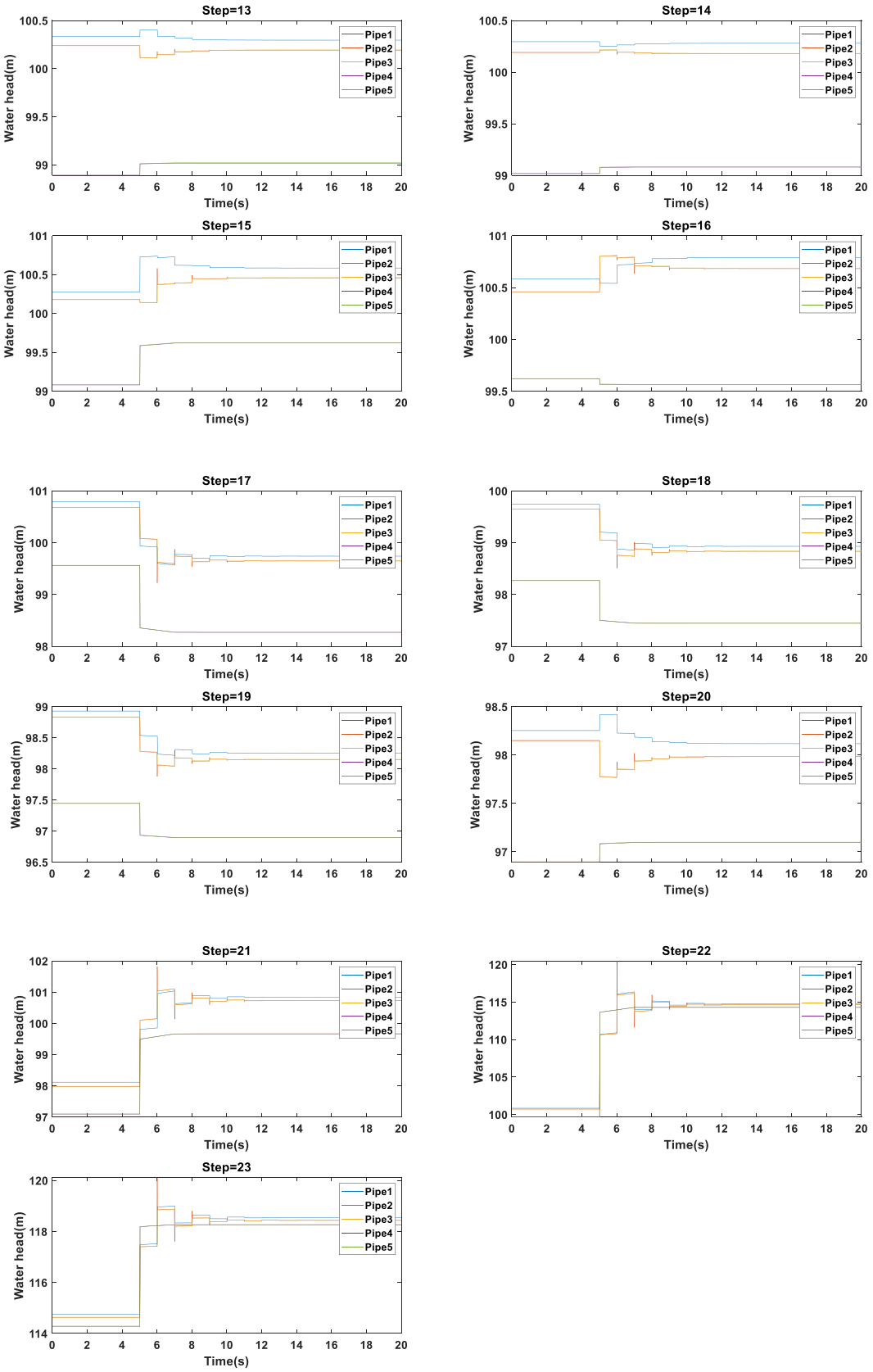

Fig. 20. (*continued*).

5. Conclusions

In this work, a bi-level quantity regulation scheduling optimization method with economic and environmental objectives for the electric-thermal integrated energy system (IES) is developed, with the considerations of thermo-hydraulic dynamic modeling of the heating subsystem. The optimization objectives are the system operation cost and carbon emission. The summarized conclusions are:

(1) The bi-level optimization method with NSGA-II and Gurobi algorithms based on quantity regulation is developed. When compared with other optimization strategy, the proposed method can obtain the Pareto frontier of the scheduling strategy more efficiently, with a computation time of 579.52 s (40% reduction) and a hypervolume of 2.0057 (1% improvement).
(2) The bi-level algorithm can achieve 100% renewable power utilization at the optimum point, when compared with 47% achieved by the single-layer algorithm. Moreover, the optimal objectives are 10150.18 U.S. dollars of operation cost and 1303.7 tons of carbon emission, while for single layer algorithm, the optimal objectives are 16776.01 U.S. dollars and 1497.6 tons, respectively.
(3) The dynamic heat transmission process of temperature response with mass flow change in the heating subsystem is considered. It is more straightforward to analyze the temperature change and time delay when using quantity regulation method instead of quality regulation method.
(4) Furthermore, the hydraulic transient process caused by the quantity regulation of heating subsystem is discussed. The hydraulic operational safety of the pipe network in the IES is within the safety threshold under the optimal scheduling strategy obtained in this work.

CRediT authorship contribution statement

Su Guo: Methodology, Writing – review & editing, Project administration, Funding acquisition. **Guotao Song:** Conceptualization, Investigation, Software, Writing – original draft, Writing – review & editing. **Mengying Li:** Validation, Supervision. **Xiaohui Zhao:** Writing – review & editing, Validation. **Yi He:** Formal analysis, Visualization. **Ainur Kurban:** Data curation. **Wenjia Ji:** Data curation. **Jiale Wang:** Data curation.

Declaration of Competing Interest

The authors declare that they have no known competing financial interests or personal relationships that could have appeared to influence the work reported in this paper.

Acknowledgements

This work is supported partially by: (1) National Key Research and Development Program of China under Grant 2018YFE0128500; (2) Open Fund of State Key Laboratory of Power Grid Security and Energy Conservation/State Grid Simulation Center (China Electric Power Research Institute) under Grant 820057016; and (3) Fundamental Research Funds for the Central Universities of China under Grant B210202069.

References

[1] Chen S, Kharrazi A, Liang S, Fath BD, Lenzen M, Yan J. Advanced approaches and applications of energy footprints toward the promotion of global sustainability. Appl Energy 2020;261:114415.
[2] Rogelj J, den Elzen M, Hohne N, Fransen T, Fekete H, Winkler H, et al. Paris Agreement climate proposals need a boost to keep warming well below 2 degrees C. Nature 2016;534:631–9.
[3] Wang D, Liu L, Jia H, Wang W, Zhi Y, Meng Z, et al. Review of key problems related to integrated energy distribution systems. CSEE J Power Energy Syst 2018;4(2):130–45.
[4] Wirtz M, Hahn M, Schreiber T, Müller D. Design optimization of multi-energy systems using mixed-integer linear programming: which model complexity and level of detail is sufficient? Energy Convers Manage 2021;240:114249. https://doi.org/10.1016/j.enconman.2021.114249.
[5] Burer S, Letchford AN. Non-convex mixed-integer nonlinear programming: A survey. Surveys Operat Res Manag Sci 2012;17(2):97–106.
[6] Kong X, Xiao J, Wang C, Cui K, Jin Q, Kong D. Bi-level multi-time scale scheduling method based on bidding for multi-operator virtual power plant. Appl Energy 2019;249:178–89.
[7] Ju L, Tan Z, Yuan J, Tan Q, Li H, Dong F. A bi-level stochastic scheduling optimization model for a virtual power plant connected to a wind–photovoltaic–energy storage system considering the uncertainty and demand response. Appl Energy 2016;171:184–99.
[8] Gu H, Li Y, Yu J, Wu C, Song T, Xu J. Bi-level optimal low-carbon economic dispatch for an industrial park with consideration of multi-energy price incentives. Appl Energy 2020;262:114276.
[9] Qu K, Shi S, Yu T, Wang W. A convex decentralized optimization for environmental-economic power and gas system considering diversified emission control. Appl Energy 2019;240:630–45.
[10] Dadashi M, Haghifam S, Zare K, Haghifam M-R, Abapour M. Short-term scheduling of electricity retailers in the presence of Demand Response Aggregators: A two-stage stochastic Bi-Level programming approach. Energy 2020;205.
[11] Li X, Wang W, Wang H. A novel bi-level robust game model to optimize a regionally integrated energy system with large-scale centralized renewable-energy sources in Western China. Energy 2021;228:120513. https://doi.org/10.1016/j.energy.2021.120513.
[12] Wang Y, Wang Y, Huang Y, Yang J, Ma Y, Yu H, et al. Operation optimization of regional integrated energy system based on the modeling of electricity-thermal-natural gas network. Appl Energy 2019;251:113410. https://doi.org/10.1016/j.apenergy.2019.113410.
[13] Wang C, Lv C, Li P, Song G, Li S, Xu X, et al. Modeling and optimal operation of community integrated energy systems: A case study from China. Appl Energy 2018;230:1242–54.
[14] Zhou J, Wu Y, Zhong Z, Xu C, Ke Y, Gao J. Modeling and configuration optimization of the natural gas-wind-photovoltaic-hydrogen integrated energy system: A novel deviation satisfaction strategy. Energy Convers Manage 2021;243.
[15] Sanaye S, Sarrafi A. Optimization of combined cooling, heating and power generation by a solar system. Renewable Energy 2015;80:699–712.
[16] Falke T, Krengel S, Meinerzhagen A-K, Schnettler A. Multi-objective optimization and simulation model for the design of distributed energy systems. Appl Energy 2016;184:1508–16.
[17] Fonseca JD, Commenge J-M, Camargo M, Falk L, Gil ID. Sustainability analysis for the design of distributed energy systems: A multi-objective optimization approach. Appl Energy 2021;290.
[18] Xu J, Wang F, Lv C, Huang Q, Xie H. Economic-environmental equilibrium based optimal scheduling strategy towards wind-solar-thermal power generation system under limited resources. Appl Energy 2018;231:355–71.
[19] Keihan Asl D, Seifi AR, Rastegar M, Mohammadi M. Multi-objective optimal operation of integrated thermal-natural gas-electrical energy distribution systems. Appl Therm Eng 2020;181:115951. https://doi.org/10.1016/j.applthermaleng.2020.115951.
[20] Algieri A, Beraldi P, Pagnotta G, Spadafora I. The optimal design, synthesis and operation of polygeneration energy systems: balancing life cycle environmental and economic priorities. Energy Convers Manage 2021;243.
[21] Wu T, Bu S, Wei X, Wang G, Zhou B. Multitasking multi-objective operation optimization of integrated energy system considering biogas-solar-wind renewables. Energy Convers Manage 2021;229:113736.
[22] Song X, Wang Y, Zhang Z, Shen C, Peña-Mora F. Economic-environmental equilibrium-based bi-level dispatch strategy towards integrated electricity and natural gas systems. Appl Energy 2021;281:116142.
[23] Zhang N, Sun Q, Yang L. A two-stage multi-objective optimal scheduling in the integrated energy system with We-Energy modeling. Energy 2021;215:119121.
[24] Wu J, Li B, Chen J, Ding Y, Lou Q, Xing X, et al. Multi-objective optimal scheduling of offshore micro integrated energy system considering natural gas emission. Int J Electr Power Energy Syst 2021;125:106535.
[25] Kuosa M, Kontu K, Mäkilä T, Lampinen M, Lahdelma R. Static study of traditional and ring networks and the use of mass flow control in district heating applications. Appl Therm Eng 2013;54:450–9.
[26] Huang W, Zhang N, Cheng Y, Yang J, Wang Y, Kang C. Multienergy networks analytics: standardized modeling, optimization, and low carbon analysis. Proc IEEE 2020;108:1411–36.
[27] Lu S, Gu W, Zhou J, Zhang X, Wu C. Coordinated dispatch of multi-energy system with district heating network: modeling and solution strategy. Energy 2018;152:358–70.
[28] Luo Xi, Liu Y, Feng P, Gao Y, Guo Z. Optimization of a solar-based integrated energy system considering interaction between generation, network, and demand side. Appl Energy 2021;294:116931.
[29] Gu W, Wang J, Lu S, Luo Z, Wu C. Optimal operation for integrated energy system considering thermal inertia of district heating network and buildings. Appl Energy 2017;199:234–46.

[30] Dancker J, Wolter M. Improved quasi-steady-state power flow calculation for district heating systems: a coupled Newton-Raphson approach. Appl Energy 2021; 295.
[31] Yao S, Gu W, Lu S, Zhou S, Wu Z, Pan G, et al. Dynamic optimal energy flow in the heat and electricity integrated energy system. IEEE Trans Sustainable Energy 2021; 12:179–90.
[32] Qin X, Sun H, Shen X, Guo Ye, Guo Q, Xia T. A generalized quasi-dynamic model for electric-heat coupling integrated energy system with distributed energy resources. Appl Energy 2019;251:113270.
[33] Mu Y, Chen W, Yu X, Jia H, Hou K, Wang C, et al. A double-layer planning method for integrated community energy systems with varying energy conversion efficiencies. Appl Energy 2020;279:115700.
[34] Wang Y, You S, Zhang H, Zheng X, Zheng W, Miao Q, et al. Thermal transient prediction of district heating pipeline: optimal selection of the time and spatial steps for fast and accurate calculation. Appl Energy 2017;206:900–10.
[35] Chen L. Simulation and application of transient flow of urban water supply pipe network; 2007.
[36] Mokryani G, Majumdar A, Pal BC. Probabilistic method for the operation of three-phase unbalanced active distribution networks. IET Renew Power Gener 2016;10: 944–54.
[37] Nazari-Heris M, Mohammadi-Ivatloo B, Gharehpetian BG. Short-term scheduling of hydro-based power plants considering application of heuristic algorithms: a comprehensive review. Renew Sustain Energy Rev 2017;74:116–29. https://doi.org/10.1016/j.rser.2017.02.043.
[38] Modern heuristic techniques for combinatorial problems, John Wiley & Sons, Inc.; 1993.